Reexamination of $M_{2,3}$ atomic level widths and $L_1M_{2,3}$ transition energies of elements $69 \leqslant Z \leqslant 95$

K. Fennane, M. Berset, J.-Cl. Dousse,* J. Hoszowska, and P.-A. Raboud
Department of Physics, University of Fribourg, CH-1700 Fribourg, Switzerland

J. L. Campbell
Guelph-Waterloo Physics Institute, University of Guelph, Guelph, Ontario, Canada N1G2W1

(Received 30 August 2013; published 11 November 2013)

We report on high-resolution measurements of the photoinduced L_1M_2 and L_1M_3 x-ray emission lines of $_{69}$Tm, $_{70}$Yb, $_{71}$Lu, $_{73}$Ta, $_{74}$W, $_{75}$Re, $_{77}$Ir, $_{81}$Tl, $_{83}$Bi, and $_{95}$Am. From the linewidths of the measured transitions an accurate set of M_2 and M_3 level widths is determined assuming for the L_1 level widths the values reported by Raboud [P.-A. Raboud *et al*.,Phys. Rev. A **65**, 022512 (2002)]. Furthermore, the present experimental $M_{2,3}$ data set is extended to $_{80}$Hg, $_{90}$Th, and $_{92}$U, using former $L_1M_{2,3}$ high-resolution x-ray emission spectroscopy measurements performed by our group. A detailed comparison of the M_2 and M_3 level widths determined in the present work with those recommended by Campbell and Papp [J. L. Campbell and T. Papp, At. Data Nucl. Data Tables **77**, 1 (2001)] and other available experimental data as well as theoretical predictions is done. The observed abrupt changes of the $M_{2,3}$ level widths versus atomic number Z can be explained satisfactorily by the cutoffs and onsets of the $M_2M_4N_1$, respectively $M_3M_4N_{3,4,5}$ and $M_3M_5N_{2,3}$ Coster-Kronig transitions deduced from the semiempirical $(Z+1)$ approximation. As a spin-off result of this study, precise L_1M_2 and L_1M_3 transition energies are obtained for the investigated elements. A very good agreement with transition energies calculated within the many-body perturbation theory is found.

DOI: 10.1103/PhysRevA.88.052506 PACS number(s): 32.70.Jz, 32.30.Rj, 32.80.Fb, 34.50.Fa

I. INTRODUCTION

Some years ago Campbell and Papp [1] presented an extensive set of K to N_7 atomic level widths for all elements across the Periodic Table, based upon a large number of literature experimental data. Their recommended M_2 and M_3 level widths were derived mostly from XPS (x-ray photoelectron spectroscopy) measurements for light elements and XES (x-ray emission spectroscopy) measurements for elements above $Z = 54$. For the XES measurements, Campbell and Papp extracted the M_2 and M_3 level widths mostly from the L_1M_2 and L_1M_3 linewidth measurements of Salem [2] and Cooper [3], assuming for the L_1 level widths their own recommended values.

More recently Raboud *et al*. [4] determined the L_1 atomic level width for several elements with atomic numbers $62 \leqslant Z \leqslant 83$ from high-resolution XES measurements of the quadrupole-allowed ($E2$) transitions $L_1M_{4,5}$, assuming for the $M_{4,5}$ level widths the values recommended by Campbell and Papp [1]. A fairly good agreement with Campbell's recommended L_1 level widths was found, except in the lanthanide region ($57 \leqslant Z \leqslant 70$) where a large discrepancy was observed. This discrepancy was explained by a splitting effect of the L_1 subshell resulting from the angular momentum coupling between the initial $2s$ vacancy and the open $4f$ subshell. This splitting effect causes an increase of the L_1 level width that was not considered in the compilation of Campbell and Papp. It was therefore concluded by Raboud *et al*. that the $M_{2,3}$ widths reported in [1] for the lanthanide region were too big. The bump occurring in the Campbell and Papp plot of the M_3 widths for $57 \leqslant Z \leqslant 70$ (see Fig. 6 of Ref. [1]) disappears if the M_3 widths in this Z region are derived using the enhanced L_1 level widths observed in [4] for the lanthanides.

It follows from the above that the question should be asked as to whether the second bump, in the Campbell and Papp M_3 plot, lying in the $75 \leqslant Z \leqslant 92$ region, is also a consequence of neglected effects within the data which are involved in deducing the M_3 width. The L_1 level widths in this region derived specifically from the L_1 Coster-Kronig and relative fluorescence yield measurements of Werner and Jitschin [5] agree with the new data of Raboud *et al*. [4], with both these sets lying significantly lower than those given in the Campbell and Papp tabulation [1]. The latter values were derived from the $L_1M_{2,3}$ measurements of Cooper [3], using the recommendations of Ref. [1] for the $M_{2,3}$ widths. One might now suspect that Cooper's $L_1M_{2,3}$ widths might also have been overestimated. Alternative values for these widths can be obtained by combining newer L_1M_3 XES measurements [5–9] and the L_1 widths from Refs. [4,10]. When this is done, the higher bump in the M_3 plot of the tabulation of Ref. [1] disappears, leaving a smooth rise instead. However, as these new XES data were scarce and strongly scattered, there appears to be strong justification in performing a new series of modern XES measurements in order to obtain a more reliable data base for the M_3 level width in the region $75 \leqslant Z \leqslant 92$.

We therefore undertook a series of high-resolution XES measurements of the L_1M_3 transitions of $_{69}$Tm, $_{70}$Yb, $_{71}$Lu, $_{73}$Ta, $_{74}$W, $_{75}$Re, $_{77}$Ir, $_{81}$Tl, $_{83}$Bi, and $_{95}$Am. As the single available L_1M_2 XES measurements in the region $75 \leqslant Z \leqslant 81$ were again those of Cooper, we decided to include in our measurements the L_1M_2 transitions. Furthermore, our experimental $M_{2,3}$ data set was extended to $_{80}$Hg, $_{90}$Th, and $_{92}$U, using former $L_1M_{2,3}$ high-resolution XES measurements performed previously by our group [8,9,11].

II. EXPERIMENT

The widths of the M_2 and M_3 atomic levels can be determined using either the $L_1M_{2,3}$ or the M_2N_4 and M_3N_5

*Corresponding author: jean-claude.dousse@unifr.ch

dipole transitions. In the Z region studied in this work, the L_1 level widths [4] as well as the N_4 and N_5 ones [1] are known with a precision better than 16%. The $N_{4,5}$ widths are, however, smaller than the L_1 ones and therefore the errors on the M_2 and M_3 level widths would be smaller if the latter were derived from the M_2N_4 and M_3N_5 transitions. Unfortunately, these M x-ray lines are about ten times less intense than the $L_1M_{2,3}$ lines and, for the studied elements, the M_3N_5 transitions are either hidden or affected by the presence of the strong L_3M_5 transitions which appear in fourth order of reflection at about the same Bragg angles as the M_3N_5 ones in first order. In addition, the line shapes of the M_2N_4 and M_3N_5 transitions are affected by partly unresolved N satellites induced by M_1M_2N and $M_{1,2}M_3N$ Coster-Kronig (CK) transitions. For these reasons, precise and reliable results cannot be obtained using these M x-ray lines. We have thus decided to measure the $L_1M_{2,3}$ transitions. A further advantage to use L_1 transitions resides in the fact that the latter are free of M- and N-shell satellites arising from CK transitions, which makes their analysis more reliable. However, due to the competitive L_1L_2X and L_1L_3X CK transitions which transfer most of the photoinduced $2s$ vacancies to the L_2 and L_3 subshells, L_1 x-ray lines are significantly weaker than L_2 and especially L_3 x-ray lines so that rather long acquisition times are required to get data with a good enough statistics. Furthermore, as the $L_1M_{2,3}$ transitions are close in energy to the strong L_2M_4 and L_3N_5 lines, not only the $L_1M_{2,3}$ transitions must be measured but all other close-lying x-ray lines. This point was found to be crucial for obtaining reliable fits of the $L_1M_{2,3}$ x-ray lines.

The measurements were performed at the University of Fribourg by means of two different high-resolution bent crystal spectrometers. For the measurements of the L x-ray spectra of $_{81}$Tl, $_{83}$Bi, and $_{95}$Am, a transmission DuMond-type crystal spectrometer was used. The latter was designed for the observation of x rays above about 11 keV. For $_{69}$Tm, $_{70}$Yb, $_{71}$Lu, $_{74}$W, $_{75}$Re, and $_{77}$Ir, the L x-ray lines were observed with a reflection von Hamos-type crystal spectrometer. Both instruments having been already described (for the DuMond spectrometer see, e.g., [8,11,12]; for the von Hamos one see [13]), only specific details concerning the setup employed in the present experiment will be given below.

A. Measurements of the elements $81 \leqslant Z \leqslant 95$

The transmission crystal spectrometer was operated in the so-called modified DuMond slit geometry. In this geometry a narrow slit located on the focal circle at a fixed position served as the effective source of radiation. The slit had a width of 0.1 mm and was made of two juxtaposed Pb plates, 25 mm high and 5 mm thick. The sample x-ray fluorescence was produced using the bremsstrahlung of a gold anode x-ray tube operated at 80 kV and 35 mA. The x-ray beam from the tube was perpendicular to the target-crystal direction. The targets were placed 1.75 cm behind the slit, at a distance of 45 mm from the tube anode, and tilted at a certain angle to the target-crystal direction. This angle was determined for each target in order to find the best compromise between two effects that modify in opposite way the intensity of the measured x rays, namely, the self-absorption of the emitted x rays in the target and the surface of the sample seen by the crystal through the slit.

For the diffraction of the fluorescent x rays, the (110) planes of a 0.5-mm-thick SiO_2 crystal were used. The 10 cm $\times$ 10 cm crystal plate was bent cylindrically to a nominal radius of 317.5 cm. The effective crystal area contributing to the diffraction of the x rays was 12 cm^2. The diffracted x rays were recorded by a 12.5-cm-diameter Phoswich scintillation detector consisting of a thin (0.63 cm) NaI(Tl) crystal followed by an optically coupled thick (5.1 cm) CsI(Tl) crystal, both crystals being mounted on the same photomultiplier. The Bragg angles were measured by means of a Doppler-shift-based optical laser interferometer with a precision of approximately 5×10^{-3} arcsec.

All samples were measured in first order of reflection. For each target, the crystal to slit distance was adjusted to obtain the best resolution and the origin of the Bragg angle scale was determined by measuring the strong L_2M_4 transition on both sides of reflection. The Tl target was prepared by rolling high-purity (99.999%) granules. The average thickness of the so-obtained foil-like Tl sample was 112 mg/cm^2. The Bi target consisted of a 25-mm-high $\times$ 5-mm-wide metallic foil, with a purity of 99.97%. Bismuth being a brittle metal, the 5-μm-thick Bi foil was mounted on a permanent polyester support. For the Am target, a ^{241}Am α-emitter source ($\sim$3 mm in diameter) was employed. The sample thickness was determined by comparing the widths of the 4.586 MeV α-particle line measured with this sample and a very thin ^{241}Am calibration source. A thickness of 1.35(25) μm was found.

For the energy calibration of the DuMond spectra, the spacing constant d_{110} of the quartz crystal was determined by assigning to the fitted peak centroid of the measured $K\alpha_1$ line of Au the reference energy taken from Deslattes and Kessler [14]. The measurements were performed in fifth order on both sides of reflection, i.e., at Bragg angles close to those corresponding to the $L_1M_{2,3}$ x- rays of the studied elements. A value $d_{110} = 2.456\,596(8)$ Å was obtained.

In the DuMond geometry the angular instrumental response does not vary in first approximation with the Bragg angle. To get a precise value for the angular instrumental broadening, measurements of the $K\alpha_{1,2}$ x-ray lines of Gd were performed in first, second, third, fourth, and fifth orders of reflection. The angular spectra were fitted with Voigt functions. Voigt profiles were chosen because they result from the convolution of the Lorentz functions representing the natural shapes of x-ray lines with the quasi-Gaussian instrumental response function of the spectrometer. The intensities, energies, Lorentzian widths, Gaussian standard deviations, and the two parameters of the linear background were let free in the fitting procedure. The weighted average of the five Gaussian standard deviations obtained from the fits was found to be $\sigma_\vartheta = 4.83(28)$ arcsec, which corresponds for the L_1M_2 and L_1M_3 transitions to instrumental energy broadenings σ_E of 1.29(7) and 1.39(8) eV for $_{81}$Tl, 1.46(8) and 1.59(9) eV for $_{83}$Bi, and 3.00(17) and 3.36(19) eV for $_{95}$Am. From the fits weighted average values of 26.1(2) and 26.4(3) eV were obtained for the Lorentzian widths of the $K\alpha_1$ and $K\alpha_2$ transitions of Gd, both results being in very good agreement with the values of 26.1(2.1) and 26.3(2.1) eV reported by Campbell and Papp [1]. To further check the goodness of the instrumental resolution measurements, the $K\alpha_1$ line of Au used for the determination of the constant d_{110} was refitted with a Voigt profile, letting free in the fitting procedure

all parameters except the Gaussian instrumental broadening which was kept fixed at the value of 8.64 eV corresponding for this transition to the above-mentioned angular resolution. From the fit, a value of 57.5(3) eV was obtained for the natural width of the Au $K\alpha_1$ transition, which is in perfect agreement with the result of 57.5(7) eV quoted in Ref. [15].

B. Measurements of the elements $69 \leqslant Z \leqslant 77$

Since the transmission-type DuMond spectrometer cannot be used for photon energies below about 11 keV, the L x-ray lines of the elements with $69 \leqslant Z \leqslant 77$ were measured with a reflection-type von Hamos bent crystal spectrometer. The principal elements of this instrument are an x-ray source defined by a rectangular slit, a cylindrically bent crystal, and a position sensitive detector located on the crystal axis of curvature. The vertical rectangular slit consists of two juxtaposed Ta plates that are 0.3 mm thick and 20 mm high. The target, crystal, and detector are all contained in a $180 \times 62 \times 25$ cm^3 stainless steel vacuum chamber, which can be pumped down to about 10^{-6} mbar in about 1 h by a turbo-molecular pump.

The fluorescence x-ray spectra were produced by irradiating the targets with the bremsstrahlung from a Cr anode x-ray tube operated typically at 60 kV and 35 mA. Each target was placed behind the slit at a distance of about 3 cm from the x-ray tube anode and tilted around a vertical axis in such a way that the normal to the sample surface made equal angles with the irradiation direction and the direction under which the sample x-ray emission was observed. A slit width of 0.2 mm was used for all samples. The emitted fluorescent x rays were diffracted by a 5-cm-wide $\times$ 10-cm-high $\times$ 0.4-mm-thick SiO_2 $(2\bar{2}3)$ crystal (spacing constant $d_{2\bar{2}3} = 1.375$ Å) bent to a radius of 25.4 cm. The diffracted x rays were detected with a 27.65-mm-long and 6.9-mm-high front-illuminated CCD (charge-coupled device) camera, having a depletion depth of 50 μm and a pixel size of 27×27 μm^2. The CCD was thermoelectrically cooled down to $-60\,^\circ$C. The targets consisted of metallic foils having a rectangular shape (20 mm high $\times$ 5 mm wide), a specified purity ranging between 99.95% and 99.99%, and thicknesses varying from 8 to 125 μm. All measurements were carried out in first order of reflection.

The energy calibration of the spectrometer was realized by measuring the $K\alpha_{1,2}$ transitions of Cu, Zn, Ge, and As and assigning to the fitted centroid positions of these lines the corresponding transition energies reported by Deslattes *et al.* [16]. These $K\alpha_{1,2}$ transitions were also employed to determine the instrumental response of the von Hamos spectrometer. The four $K\alpha_{1,2}$ lines were fitted with Voigt profiles. The Lorentzian natural widths were kept fixed in the fits at the values derived from the atomic level widths reported in Ref. [1] but the instrumental Gaussian broadenings were let free. For the latter, standard deviations σ_E of 0.96(5) eV at 8048 eV (Cu), 1.29(5) eV at 8638 eV (Zn), 1.71(6) eV at 9886 eV (Ge), and 1.83(8) eV at 10543 eV (As) were obtained from the fits. The uncertainties on the atomic level widths quoted in [1] were taken into account in the determination of the errors $\Delta\sigma_E$. The instrumental broadenings corresponding to the L x-ray lines of interest were then calculated by interpolation, using the four above-mentioned values σ_E.

Since in the present experiment the measurements were performed by means of two different spectrometers whose energy domains are partly overlapping, we found it useful to measure one transition with both instruments in order to probe the accuracy and reliability of our results. For this reason, the L_1M_3 transition of the lightest element measured with the DuMond spectrometer (i.e., $_{81}$Tl) was also measured with the von Hamos spectrometer. The same SiO_2 $(2\bar{2}3)$ crystal was employed but as the minimum Bragg angle that can be measured with the von Hamos spectrometer amounts to about 24°, which corresponds in first order to a maximum energy of about 11.1 keV, the $_{81}$Tl L_1M_3 transition ($E \cong 12.4$ keV) had to be measured in second order of reflection. For this line, the energy calibration and the instrumental response of the von Hamos spectrometer were determined by measuring in second order the $K\alpha_{1,2}$ transitions of Se and gaseous Kr, using again for the reference energies and natural linewidths the values quoted in Refs. [16] and [1]. Instrumental broadenings of 1.45(10) and 2.50(9) eV were found for Se and Kr, respectively. As shown later (see Sec. IV) nearly consistent results were obtained for the energy and consistent results for the width of the L_1M_3 transition of Tl but the uncertainties of the results obtained with the von Hamos spectrometer are rather large due to the poor statistics of this measurement performed in second order of reflection.

III. DATA ANALYSIS

As mentioned before, in order to obtain reliable results, not only the $L_1M_{2,3}$ transitions of interest had to be measured but also several neighboring transitions so that for all samples rather broad energy domains should be scanned. However, because for measurements performed with the DuMond spectrometer the x-ray spectra are measured point by point, the times needed to measure such broad spectra would have been very long. In addition, as the absorption in the crystal is rather strong for low photon energies as those corresponding to the $L_1M_{2,3}$ transitions, rather long acquisition times per point are needed to get data with a good enough statistics. For these reasons, the Tl and Bi measurements were performed in the following way: In a first stage, the chosen energy domains (11764–12558 eV for Tl and 12370–13307 eV for Bi) were scanned with reasonably long acquisition times, namely, 450 and 300 s per point, respectively. In a second stage, narrower energy domains corresponding to the L_1M_2 and L_1M_3 transitions only were measured in several successive scans. The different scans were then summed together off-line leading to total acquisition times of 1800 and 1350 s per point, respectively, for the L_1M_2 and L_1M_3 transitions of Tl, and correspondingly 1100 and 600 s per point for Bi. In the fits of the L_1M_2 and L_1M_3 lines obtained from the sum of the different scans, the linear background and the parameters of the neighboring lines (intensities, centroid energies, widths) were kept fixed at the values obtained from the analysis of the broad spectra, values normalized beforehand for the acquisition time differences. For Am, only the L_1M_2 and L_1M_3 transitions of interest were measured, because in this case there is no strong line close in energy that may influence the widths of the $L_1M_{2,3}$ transitions. As the thickness of the employed Am target was very small, which resulted in poor intensities for the $L_1M_{2,3}$

transitions, the latter were also measured in several successive scans corresponding to total acquisition times per point of 8800 and 7000 s for the L_1M_2 and L_1M_3 transitions, respectively.

For the measurements performed with the von Hamos spectrometer, energy domains of about 600 eV had to be measured to include the neighboring lines. For a given position of the crystal and detector the von Hamos geometry permits data acquisition over an energy bandwidth which is limited by the detector length [13]. For the same energy interval, measurements performed with the von Hamos spectrometer are therefore usually shorter than those performed with the DuMond spectrometer. Depending on the central Bragg angle and the employed crystal, the covered energy interval varies between 30 and 300 eV. For the present project, the width of the energy interval was about 200 eV so that at least three different positions of the crystal and detector were needed. Actually, in order to have some overlap between the adjacent spectra, for each sample four partial spectra were measured. The intensities of the partial spectra were normalized off-line, using the intensity ratios between the overlapping energy regions, and the four spectra were then put together.

Except for Am, for which only the $L_1M_{2,3}$ transitions were observed, the energy domains measured with the two spectrometers contained the transitions L_1M_2, L_3N_1, L_2M_4, L_1M_3, L_3N_4, and L_3N_5, and the M satellites of the $L_3N_{4,5}$ transitions. For Tl and Bi, the $L_3N_{6,7}$ transitions were also observed. As the energies of the diagram transitions depend on the target element, the above-mentioned sequence of transitions was not the same for each sample. All spectra were analyzed by means of a least-squares-fitting program, employing Voigt profiles to fit the transitions. In the fitting procedure, the natural widths of the L x-ray lines were extracted by keeping the Gaussian instrumental broadenings fixed at their known values. The energies and the intensities of the transitions as well as a linear background were used as additional free fitting parameters. The x-ray lines measured with the von Hamos spectrometer were found to exhibit a small asymmetry on their low-energy flank. This asymmetry, which originated from the crystal, was investigated carefully and its variation with energy determined accurately. In the fits, the asymmetry was accounted for by adding a Voigtian on the low-energy side of all transitions. For illustration, the fitted high-resolution L x-ray spectrum of $_{70}$Yb measured with the von Hamos spectrometer and the one of $_{81}$Tl measured with the DuMond spectrometer are depicted in Figs. 1 and 2, respectively.

The $L_3N_{4,5}$ lines of $_{73}$Ta, $_{75}$Re, $_{77}$Ir, $_{81}$Tl, and $_{83}$Bi evince asymmetries on their high-energy sides due to the presence of unresolved N spectator holes. Actually the energy shifts of satellites relative to the parent diagram lines increase with the principal quantum number of the transition electron and decrease with the principal quantum number of the spectator vacancy. As a result, for L x rays, the N x-ray satellites in most cases cannot be resolved from their parent diagram lines because their energy shifts are smaller than the natural linewidths of the transitions and the N spectator holes lead only to broadenings or asymmetries of the diagram lines. In contrast to that, M satellites are generally well resolved. In the present project, the M satellites of the $L_3N_{4,5}$ transitions were observed for almost all studied elements, whereas those

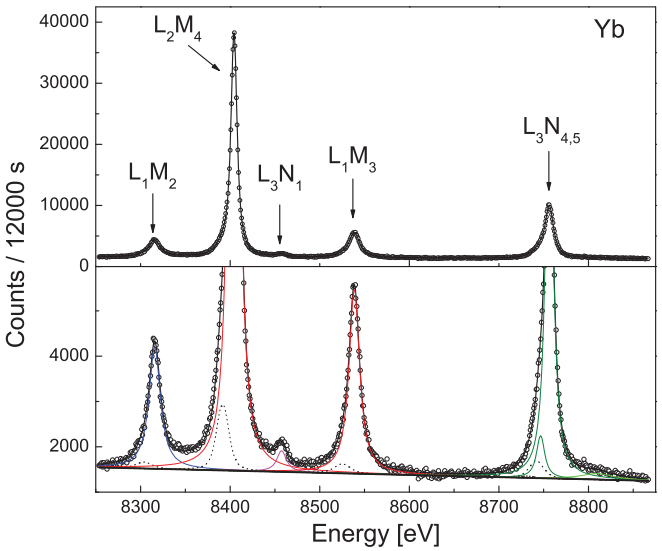

FIG. 1. (Color online) High-resolution L x-ray spectrum of Yb measured with the von Hamos spectrometer. The top part of the figure presents the total fit of the spectrum; the bottom part shows details about the fitted components. The dotted lines represent the Voigtians used in the fit to account for the crystal asymmetry. The line observed at about 8810 eV corresponds to the M satellite of the $L_3N_{4,5}$ transitions.

of the L_3N_1 transitions were not seen, their intensities being negligibly small. M satellites of the strong L_2M_4 transitions were also observed in the spectra of $_{73}$Ta, $_{74}$W, $_{75}$Re, and $_{77}$Ir. Since L_1L_2M CK transitions are energetically forbidden for these elements, the weak M satellites are probably due to M-shell shake processes following the photoinduced production of the $2s$ core vacancy.

In $_{69}$Tm, $_{71}$Lu, $_{73}$Ta, $_{74}$W, $_{75}$Re, and $_{77}$Ir, small asymmetries were observed on the low-energy sides of the L_2M_4 transition.

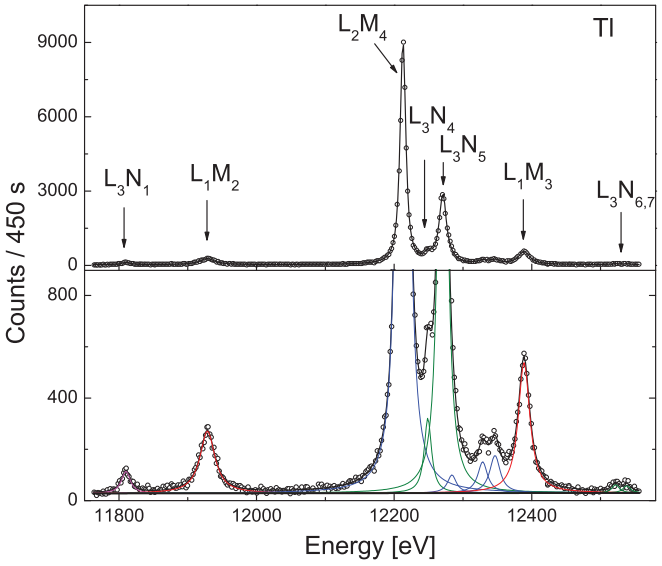

FIG. 2. (Color online) Same as Fig. 1 but for Tl. The spectrum was measured with the Dumond spectrometer. The lines observed at 12 290, 12 329, and 12 347 eV correspond to the M satellites of the $L_3N_{4,5}$ transitions.

These asymmetries, which result from the angular momentum coupling between the L_2 core vacancy and the partially filled outer shells, were accounted for in the fits by adding one or two additional Voigt functions. For Yb ([Xe]$4f^{14}6s^2$), no asymmetry was observed since in the Yb crystal the two $6s$ electrons participate in the crystal bonding, leaving the atom with a closed electronic shell configuration [17]. The same holds for Tl ([Hg]$6p$) and Bi ([Hg]$6p^3$) which are generally monovalent and trivalent, respectively. For Ir the L_1M_2 and L_3N_1 transitions are strongly overlapping. Any attempt to let free in the fitting procedure the energy and linewidth of the L_3N_1 line was found to be unsuccessful, and hence these two parameters were kept fixed at the values taken from Refs. [16] and [1], respectively.

IV. RESULTS AND DISCUSSION

A. $L_1M_{2,3}$ transition energies

The energies of the measured $L_1M_{2,3}$ transitions are given in Table I together with the experimental and theoretical values reported by Deslattes *et al*. [16]. As shown, present results are all consistent within the combined errors with the theoretical transition energies quoted in [16]. The uncertainties given for the latter are rather large (about 3 eV) so that the observed overall agreement is not really surprising. Nevertheless, we would like to point out that the average value of the differences between our results and these theoretical predictions is only 0.8 eV, i.e., about four times less than the errors quoted for the theoretical values. In contrast to that, about 35% of the experimental values listed in [16] are not consistent with our results, the biggest deviation being observed for the L_1M_3 transition of Tm (difference of 2.8 eV significantly bigger than the quoted error of 1.6 eV). It should be noted, however, that for the considered elements all experimental values reported in [16] were taken from the prior tabulation of Bearden [18]. Although these old Bearden's data were readjusted in [16] to the new x-ray wavelength scale, they have to be regarded cautiously because several modern x-ray metrology measurements have shown that Bearden's values deviate sometimes from the new results by several standard deviations, especially for weak x-ray lines. For instance, for the above-mentioned L_1M_3 transition of Tm, the Bearden's value looks dubious since it is 3.4 eV smaller than the corresponding theoretical prediction, whereas for the L_1M_2 transition of the same element the difference with theory is only 0.3 eV.

For the measurements performed with the von Hamos spectrometer, the errors of present results originate mainly from the energy calibration procedure (see Table I). In general, the energy uncertainty of transitions observed with the von Hamos spectrometer increases with the difference between the Bragg angles corresponding to the transition of interest and the transition employed as reference for the energy calibration. For instance, for Ir which was calibrated with the $K\alpha_1$ transition of As ($E = 10\,543.2674 \pm 0.0081$ eV [16]), the energy calibration error of the L_1M_2 transition is only 0.03 eV because the Bragg angles corresponding to the two transitions differ by less than 0.09°, whereas for the L_1M_3 transition, due to the bigger difference in the Bragg angles (0.8°), the calibration error is approximately seven times bigger (0.20 eV). A further contribution to the relatively big energy calibration errors affecting the von Hamos measurements originates from the uncertainties on the energies of the transitions used as references. For the L_1M_3 transition of W which was calibrated with the $K\alpha_1$ transition of Ge, the calibration error is 0.11 eV although the two Bragg angles are similar (difference smaller than 0.2°) because the energy of the $K\alpha_1$ transition of Ge is only known with a moderate precision ($E = 9886.52 \pm 0.11$ eV [16]).

For the measurements performed with the DuMond spectrometer, quoted errors arise mainly from the fitting procedure, the uncertainty related to the energy calibration being small (0.04–0.06 eV). For Am, despite the long acquisition times used to measure the two transitions (about 170 h for the L_1M_2 transition and about 130 h for the L_1M_3), the errors given by

TABLE I. Energies of the L_1M_2 and L_1M_3 transitions. Present results are compared to experimental and theoretical values reported by Deslattes *et al*. [16]. The notation 8025.10(10/13) eV means 8025.10 ± 0.13 eV with an included contribution of ± 0.10 eV from the uncertainty related to the energy calibration of the spectrometer. Elements with $69 \leqslant Z \leqslant 77$ were measured with the von Hamos spectrometer; those with $81 \leqslant Z \leqslant 95$ with the DuMond spectrometer. The L_1M_3 line of $_{81}$Tl was measured with both spectrometers.

	L_1M_2 transition energy (eV)			L_1M_3 transition energy (eV)		
	Experiment		Theory	Experiment		Theory
Element	This work	Ref. [16]	Ref. [16]	This work	Ref. [16]	Ref. [16]
$_{69}$Tm	8025.10(10/13)	8025.8(1.5)	8026.1(2.6)	8233.75(11/13)	8230.9(1.6)	8234.2(2.6)
$_{70}$Yb	8313.36(42/43)	8313.26(25)	8313.6(2.7)	8356.17(42/43)	8536.79(43)	8536.8(2.8)
$_{71}$Lu	8607.74(27/28)	8606.54(44)	8606.3(2.7)	8846.73(28/29)	8847.03(47)	8845.6(2.7)
$_{73}$Ta	9212.82(30/31)	9212.47(30)	9212.6(2.7)	9487.50(23/24)	9487.62(32)	9487.1(2.8)
$_{74}$W	9526.20(21/23)	9525.23(54)	9526.0(2.8)	9819.95(12/13)	9818.91(46)	9819.5(2.9)
$_{75}$Re	9847.05(11/14)	9846.35(58)	9846.8(2.8)	10160.29(19/20)	10159.90(62)	10160.4(2.9)
$_{77}$Ir	10510.42(3/11)	10510.72(40)	10510.4(2.9)	10866.59(20/21)	10866.54(42)	10867.5(3.0)
$_{81}$Tl	11929.68(4/14)	11930.78(51)	11931.0(3.0)	12390.33(25/70)[a] 12389.40(4/9)[b]	12390.55(55)	12390.6(3.2)
$_{83}$Bi	12690.58(4/8)	12691.40(77)	12690.9(3.1)	13209.57(4/9)	13209.99(62)	13210.4(3.2)
$_{95}$Am	18063.35(6/34)	18062.96(78)	18065.7(3.5)	19104.98(6/40)	19106.24(87)	19107.4(3.7)

[a]von Hamos.
[b]DuMond.

TABLE II. Spin-orbit splitting energies in eV between the $3p_{3/2}$ and $3p_{1/2}$ atomic levels. Present experimental results are compared to theoretical predictions from MBPT and multiconfiguration DF calculations.

Element	This work	MBPT [16]	DF [19]
$_{69}$Tm	208.65(18)	208.2	211.2
$_{70}$Yb	222.81(61)	223.2	226.6
$_{71}$Lu	238.99(40)	239.3	242.9
$_{73}$Ta	274.68(39)	274.5	278.6
$_{74}$W	293.75(26)	293.5	297.7
$_{75}$Re	313.24(24)	313.6	318.0
$_{77}$Ir	356.17(24)	357.1	362.2
$_{81}$Tl	459.72(17)	459.6	466.0
$_{83}$Bi	518.99(26)	519.5	526.6
$_{95}$Am	1041.63(52)	1041.7	1055.7

the fits were rather large (0.33 and 0.40 eV, respectively). The poor statistics of these measurements resulted mainly from the tiny dimensions of the employed sample. The effective surface of the latter was indeed only about 7 mm^2 (125 mm^2 for Th and Bi) and its thickness 1.35 μm.

The $3p$ spin-orbit splitting energies were derived from the energy differences between the L_1M_3 and L_1M_2 transitions. Results are presented in Table II where they are compared to theoretical predictions obtained from many-body perturbation theory calculations (MBPT) [16] and relativistic Dirac-Fock calculations (DF) [19]. As shown, present results agree very well with predictions from MBPT calculations since an average deviation smaller than 0.4 eV is observed. On the contrary, DF calculations seem to systematically overestimate our values by approximately 1.5%. The energy difference between the M_3 and M_2 levels can also be derived from the separation energy between the $K\beta_1$ and $K\beta_3$ x-ray lines. For tungsten, Kessler *et al*. [15] have reported for these transitions energies of 67 245.45 and 66 952.40 eV. The precision of the measurements was 16 ppm. From these values an energy difference of 293.05 $\pm$ 1.52 eV is found, which is also in good agreement with the result of 293.75 $\pm$ 0.26 eV obtained from our measurements.

As mentioned in Sec. II the L_1M_3 transition of Tl was measured with both the DuMond and von Hamos spectrometers. As shown in Table I, the obtained energies are nearly consistent, a difference of 0.93 eV being observed which is 30% bigger than the error of 0.70 eV given for the von Hamos measurement. Note that this error is much bigger than the one corresponding to the measurement performed with the DuMond spectrometer because of the poor statistics of the von Hamos measurement. The latter indeed had to be performed in second order of reflection, which resulted in a significant loss of the crystal reflectivity. In addition, for this relatively high energy (12.4 keV), the CCD efficiency was smaller than for other lighter elements. Finally, the L_1M_3 transition of Np was observed in the L_1M_2 spectrum of Am (see Fig. 3). An energy of 17 993.9 eV was found for this transition. However, as the Np L_1M_3 line is still weaker than the L_1M_2 line of Am and partly overlapping with the latter, the error of $\pm$4.7 eV given by the fit was so large that we preferred not to include this transition in Table I.

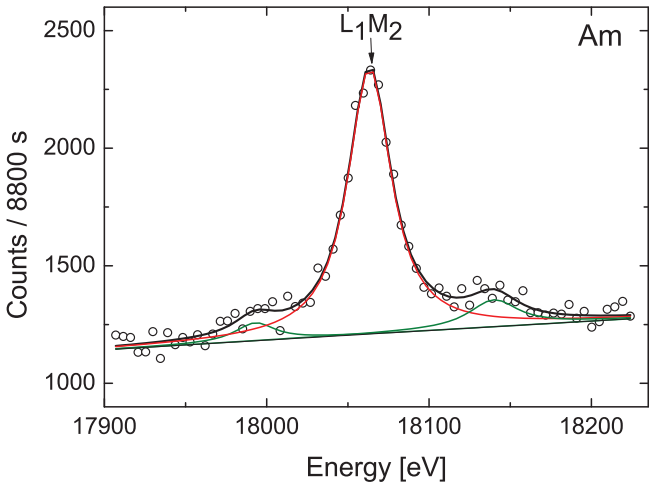

FIG. 3. (Color online) L_1M_2 x-ray line of Am measured with the DuMond spectrometer. The line observed at about 18 140 eV corresponds to the L_3O_1 transition and the one at about 17 990 eV to the L_1M_3 transition of $^{237}_{93}$Np which results from the α decay of $^{241}_{95}$Am.

B. $L_1M_{2,3}$ transition widths

The L_1M_2 and L_1M_3 linewidths obtained in the present work are presented in Table III. For comparison, the corresponding recommended values of Campbell and Papp [1] and theoretical predictions by Perkins *et al*. [20] are also listed. These data and other earlier experimental values are also represented graphically in Figs. 4 and 5. As shown, except for Bi, present L_1M_2 transition widths are systematically bigger (10%–20%) than the values recommended by Campbell and Papp. For the L_1M_3 transitions, the same trend is observed but only for the elements $Z \leqslant 75$.

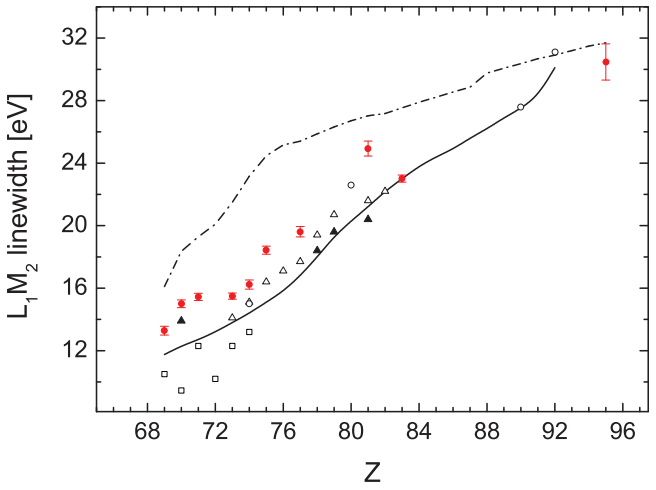

FIG. 4. (Color online) Linewidth of the L_1M_2 transition versus atomic number. The solid line represents the recommended values of Campbell and Papp [1], the dash-dotted line the calculations of Perkins [20], and the red full circles the results obtained in the present work. Other plotted experimental data were taken from Ref. [2] (open squares), Ref. [3] (open triangles), Ref. [21] (full triangles), and Refs. [6,8,9,11] (open circles).

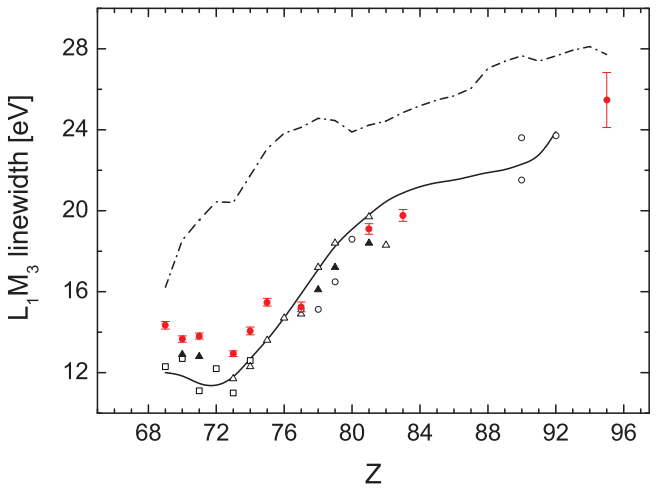

FIG. 5. (Color online) Linewidth of the L_1M_3 transition versus atomic number. The same symbols as in Fig. 4 are used except for the experimental data represented by the open circles which were taken from Refs. [5–9,11].

From Table III, it can be seen that for both spectrometers total errors arise mainly from the statistical errors given by the fits, the contribution of the errors from the instrumental broadening being negligible in most cases. The widths of the L_1M_3 transitions of Tl measured with the DuMond and von Hamos spectrometers are in good agreement since they differ only by 0.3 eV, the error in the result obtained with the von Hamos spectrometer being seven times bigger (2.1 eV). As for the energy, this important error of 2.1 eV is due to the poor statistics of the measurement which was performed in second order of reflection.

Only three relatively recent data are available for comparison with the widths obtained in the present work. The first one concerns Ir, for which a width of 15.1 ± 0.5 eV, in fairly good agreement with our result of 15.25 ± 0.25 eV, is reported in [7] for the L_1M_3 transition. The two other available data concern the L_1M_2 and L_1M_3 widths of W for which values of 15.0 ± 0.5 eV and 12.7 ± 0.5 eV are quoted in [6]. The latter are both smaller than ours by 10% and 8%, respectively. A possible explanation for the slight discrepancy is that the instrumental broadening in [6] was somewhat overestimated. To extend the comparison to other elements, linear interpolations of the measured transition widths were done in two separate segments of atomic number, viz., Ir-Tl and Bi-Am. From these interpolations, values of 23.6(4) and 18.1(3) eV, 27.4(8) and 22.6(9) eV, and 28.6(9) and 23.4(1.1) eV were obtained for the widths of the L_1M_2 and L_1M_3 transitions of Hg, Th, and U. Keeping in mind that above interpolations represent rather crude approximations for the real transition widths, the obtained values can be considered to be again in quite satisfactory agreement with the widths of 22.6(3) and 18.6(3) eV, 27.6(7) and 23.6(3) eV, and 31.1(3) and 23.7(4) eV reported for Hg [11], Th [9], and U [8].

C. $M_{2,3}$ level widths

The energy width of an atomic level is related to the lifetime of the vacancy created in that level by the Heisenberg's uncertainty principle. The primary vacancy can be filled as a result of a radiative, Auger or CK transition. For M levels, the fluorescence yields are small (less than 5.5% for the Z region studied in this work [22,23]). As a consequence, the total M level widths are almost entirely due to nonradiative decay processes. According to Coster and Kronig [24], the probability of an Auger transition is proportional to the overlap between the wave functions of the initial and final states of both the transition electron and the ejected electron. Therefore, when they are energetically allowed, CK and especially super CK transitions (i.e., CK transitions involving three subshells of the same major shell) are highly probable and the level widths are governed mainly by these transitions. For the Z region concerned by this study, super CK transitions are energetically forbidden but there are several allowed CK transitions and the $M_{2,3}$ level widths are mostly due to them. In $_{74}$W for example,

TABLE III. Natural linewidths in eV of the L_1M_2 and L_1M_3 x-ray transitions. Our experimental results are compared to the recommended values of Campbell and Papp [1] and to theoretical predictions of Perkins *et al*. [20]. The notation 13.28(5/28) eV means 13.28 ± 0.28 eV with an included contribution of ± 0.05 eV from the instrumental broadening uncertainty.

	Experiment				Theory	
	Present		Campbell [1]		Perkins [20]	
Element	L_1M_2 width	L_1M_3 width	L_1M_2 width	L_1M_3 width	L_1M_2 width	L_1M_3 width
$_{69}$Tm	13.28(5/28)	14.34(5/19)	11.8(1.7)	12.0(1.7)	16.1	16.2
$_{70}$Yb	15.0(5/25)	13.66(5/16)	12.3(1.8)	11.9(1.7)	18.4	18.5
$_{71}$Lu	15.44(5/23)	13.81(6/15)	12.7(1.8)	11.4(1.7)	19.3	19.5
$_{73}$Ta	15.49(6/20)	12.94(8/14)	13.8(1.9)	11.7(1.7)	21.5	20.4
$_{74}$W	16.23(7/29)	14.06(8/19)	14.4(1.9)	12.7(1.8)	23.2	27.7
$_{75}$Re	18.43(7/26)	15.48(9/19)	15.1(2.0)	13.6(1.9)	24.5	23.1
$_{77}$Ir	19.61(7/33)	15.25(12/24)	16.8(2.5)	13.6(1.9)	25.4	24.1
$_{81}$Tl	24.93(4/48)	19.40(12/2.15)[a] 19.10(6/26)[b]	21.2(2.8)	19.8(2.6)	27.0	24.2
$_{83}$Bi	23.01(6/23)	19.77(8/29)	23.0(2.9)	20.9(2.6)	27.5	24.9
$_{95}$Am	30.47(11/1.16)	24.59(13/1.37)			31.7	27.7

[a]von Hamos.
[b]DuMond.

TABLE IV. $M_{2,3}$ atomic level widths. Present results were deduced from the transition widths quoted in Table III and the L_1 level widths reported in [4] or interpolated from the latter. For comparison the L_1 and $M_{2,3}$ widths recommended by Campbell and Papp [1] and theoretical $M_{2,3}$ widths of Perkins *et al.* [20] are also indicated. All widths are given in eV.

	Experiment						Theory	
	Raboud [4]	Campbell [1]	Present		Campbell [1]		Perkins [20]	
Element	L_1 width	L_1 width	M_2 width	M_3 width	M_2 width	M_3 width	M_2 width	M_3 width
$_{69}$Tm	5.45(32)	4.9(1.5)	7.83(43)	8.89(37)	6.9(9)	7.1(9)	9.9	10.1
$_{70}$Yb	5.40(30)	5.2(1.5)	9.60(39)	8.26(34)	7.1(9)	6.7(9)	10.3	10.5
$_{71}$Lu	5.65(33)	5.4(1.5)	9.79(40)	8.16(36)	7.3(1.0)	6.0(8)	10.6	10.9
$_{73}$Ta	6.16(40)	6.0(1.5)	9.33(45)	6.78(42)	7.8(1.1)	5.7(8)	10.3	10.2
$_{74}$W	6.41(43)	6.3(1.5)	9.82(52)	7.65(47)	8.1(1.2)	6.4(1.0)	11.5	10.1
$_{75}$Re	6.94(50)	6.7(1.5)	11.49(56)	8.54(53)	8.4(1.3)	6.9(1.1)	11.8	10.4
$_{77}$Ir	8.02(63)	7.9(2.0)	11.59(71)	7.23(67)	8.9(1.5)	8.0(1.4)	12.3	11.0
$_{81}$Tl	11.28(68)	11.1(2.0)	13.65(83)	7.82(73)	10.1(1.9)	8.7(1.7)	13.1	10.3
$_{83}$Bi	12.50(45)	12.3(2.0)	10.51(51)	7.27(54)	10.7(2.2)	8.6(1.7)	13.5	10.8
$_{95}$Am	16.63(30)		13.84(1.20)	7.96(1.40)			15.5	11.5

the calculations of Perkins [20] suggest that 77% of the M_2 vacancies and 70% of the M_3 vacancies are filled through CK transitions. Since the differences between the electron binding energies in the subshells vary with the atomic number Z, certain CK transitions exist only for elements belonging to specific Z regions of the Periodic Table [25]. The first element for which a given CK transition becomes energetically allowed or forbidden is called the onset or cut-off element for the considered CK transition.

Auger and Coster-Kronig transition probabilities for the $M_{2,3}$ subshells of elements with atomic numbers $22 \leqslant Z \leqslant 90$ were calculated by McGuire using a nonrelativistic Herman and Skillman potential and a semiempirical estimation for the transition energies [21]. Chen *et al.* [22] reported relativistic calculations of nonradiative rates for the $M_{1,2,3}$ subshells of ten elements with $67 \leqslant Z \leqslant 95$ based on Dirac-Hartree-Slater (DHS) wave functions. Using the results of Scofield's DHS calculations for the radiative rates [26], they also computed the total $M_{1,2,3}$ level widths. Their results were found to overestimate the experimental data but showed a significant improvement with respect to the nonrelativistic calculations of McGuire. A much better agreement with experimental data was obtained by Ohno *et al.* [27] from MBPT calculations. However, these calculations were performed only for elements $36 \leqslant Z \leqslant 54$. An extension of both the DHS relativistic calculations of Chen [22] for the nonradiative rates and those of Scofield [26] for the radiative rates to all elements in the range $1 \leqslant Z \leqslant 100$ was reported later by Perkins *et al.* [20].

In the present work, the natural widths of the M_2 and M_3 subshells were determined from the differences between the measured widths of the $L_1M_{2,3}$ transitions and the experimental widths of the L_1 subshell reported by Raboud *et al.* in [4]. Raboud's results were preferred to Campbell's recommended values because the latter have error estimates three to five times bigger than the ones of Raboud. For the elements that were not measured in [4], linear interpolations between the two next-neighboring elements with Z below and above the atomic number of the element of interest were employed. For Tm, the L_1 width was taken from the curve given by Raboud *et al.* for the lanthanide region (see Fig. 5 of Ref. [4]). In this region, a broadening of the $2s$ level was indeed observed. The latter was explained by a splitting effect of the L_1 subshell due to an exchange interaction between the spin of the $2s$ level and the total spin of the unfilled $4f$ level. Similar effects were observed for the $4s$ and $5s$ levels of rare earths [28] and, more recently, for the $3s$ level [17]. For Am, the L_1 width was determined by a linear extrapolation of the values reported in [4] for Bi and in [9] for Th and U.

The M_3 level widths obtained in this work are presented in Table IV together with the recommended values of Campbell and Papp [1] and the theoretical predictions of Perkins *et al.* [20]. Values of the L_1 widths from [4] and [1] are also listed. A graphical comparison between present results and other available experimental and theoretical data is given in Fig. 6.

The broken curve in Fig. 6 corresponds to Perkins total M_3 level widths obtained by summing his computed radiative and nonradiative rates. The puzzling variations observed in this curve are fully accounted for by the changes in the probabilities of the CK transitions listed in Ref. [20]. The drop around $Z = 74$ is due to the closing of the $M_3M_4N_3$ and $M_3M_5N_2$ CK channels while the drops occurring at $Z = 80$, 86, 91, and 95 are due, respectively, to the closing of the $M_3M_5N_3$, $M_3M_4N_{4,5}$, and $M_3M_5N_{4,5}$ channels. The solid curve in Fig. 6 corresponds to the M_3 level widths recommended by Campbell and Papp. The latter were obtained by subtracting their own recommended L_1 level widths from the L_1M_3 XES measurements of Salem [2] in the Z region $58 \leqslant Z \leqslant 72$, those of Cooper [3] in the Z region $73 \leqslant Z \leqslant 81$, and those performed previously by our group for $_{90}$Th [9] and $_{92}$U [8]. As noted by Campbell and Papp in Ref. [29], for the three elements $_{78}$Pt, $_{79}$Au, and $_{81}$Tl, there are discrepancies between Cooper's data published in 1942 [30] (open triangles in Fig. 6) and those published in 1944 [3] (full triangles in Fig. 6). However, because there were no other available data, the M_3 level widths recommended in Ref. [1] were extracted from the later Cooper data, i.e., those of 1944.

As shown in Fig. 6, in the region $69 \leqslant Z \leqslant 74$, our results (red full circles) exceed those of Salem and Lee [2], suggesting the possibility that the M_3 level widths extracted from L_1M_3 linewidth measurements of Salem and Lee for lower atomic

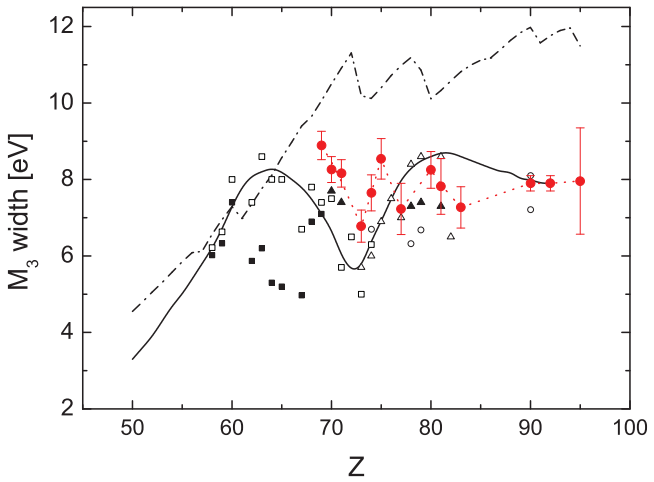

FIG. 6. (Color online) M_3 level width versus atomic number. The dash-dotted line represents the independent particle model calculations of Perkins *et al*. [20] and the solid line the recommended values of Campbell and Papp [1]. Experimental data were derived from L_1M_3 XES measurements using present data and former ones of the Fribourg group [8,9,11] (red full circles) as well as data from Refs. [5–7] (open circles), Ref. [3] (open triangles), Ref. [30] (full triangles), and Ref. [2] assuming the L_1 widths from [4] (open squares) and [1] (full squares), respectively. The red dotted line serves only to guide the eye.

numbers ($58 \leqslant Z \leqslant 68$) might also be too low. Our data lie also systematically above those of Cooper [30]. However, as already reported in [31], Cooper's data were probably overcorrected for the instrumental response. Furthermore, it can be seen in Fig. 6 that all experimental data lie significantly lower than the Perkins theoretical predictions [20]. Actually, Perkins himself mentioned that his computed CK transition rates may overestimate the true values by a factor up to 2 due to the small binding energy differences. This was also pointed out by Campbell and Papp [1,29] who observed that Perkins calculations largely exceed the experimental widths for all levels dominated by CK decay, while they provide a fairly good approximation for other levels.

Finally, it can be noted that our experimental values reveal oscillations similar to those observed in Perkins curve. However, they do not peak at the same atomic numbers, indicating that the CK cut-off atomic numbers derived from the present measurements do not correspond to those predicted by Perkins calculations. Table V presents the cut-off atomic numbers deduced from our measurements, those predicted by Perkins, and those from the $(Z + 1)$ approximation using the experimental binding energies tabulated by Storm and Israel [32]. The $(Z + 1)$ approximation appears to provide cut-off atomic numbers that are in better agreement with our experimental data than those deduced from Perkins calculations which yield systematically higher values. This may indicate that Perkins calculations overestimate the CK transition energies. Similar observations were made by Campbell for the $M_4M_5N_{4,5}$ CK transitions. For the latter Perkins indeed predicts the onset at $Z = 49$, while Martensson [33] measured a maximum rate for $_{44}$Ru and $_{45}$Rh and the cutoff at $Z = 47$. Similarly, for the $L_2L_3M_5$ and $L_2L_3M_4$ CK transitions, the onsets are

TABLE V. Cut-off atomic numbers of the $M_3M_4N_{3-5}$ and $M_3M_5N_{2-5}$ CK transitions. The cut-off element uncertainty $\Delta Z = 1$ of this work is related to the fact that the elements $_{72}$Hf, $_{76}$Os, and $_{82}$Pb were not measured.

CK transition	This work	$(Z + 1)$ approx.	Perkins [20]
$M_3M_5N_2$	72 or 73	71	73
$M_3M_4N_3$	72 or 73	72	74
$M_3M_5N_3$	76 or 77	77	80
$M_3M_4N_4$	82 or 83	83	85
$M_3M_4N_5$	82 or 83	84	86
$M_3M_5N_4$		89	91
$M_3M_5N_5$		91	95

predicted by Perkins at $Z = 88$ and $Z = 91$, respectively, whereas measurements of L_2L_3 CK transition probabilities show onsets at $Z = 92$ and $Z = 94$. Note that for these three CK transitions, the $(Z + 1)$ approximation provides a good agreement with experiment ($Z = 47$ for the cutoff of the $M_4M_5N_{4,5}$ transition and $Z = 91$ and 93, respectively, for the onsets of the $L_2L_3M_5$ and $L_2L_3M_4$ transitions). The drop in the M_3 level width corresponding to the closing of the $M_3M_4N_{4,5}$ CK channels is much more pronounced in our experimental data indicating that Perkins predictions probably underestimate the rates of these CK transitions. Concerning the closing of the $M_3M_5N_{4,5}$ CK channel, no clear conclusion could be deduced from Fig. 6, the error on the M_3 level width of Am obtained in this work being too large.

Present results for the M_2 level widths are presented in Table IV and in Fig. 7 where they are compared to other existing experimental and theoretical data. In general, similar conclusions as those given for the M_3 level widths can be drawn. Except for Bi, present results are indeed bigger by about 30% than the values recommended by Campbell and Papp and smaller than Perkins theoretical predictions.

In Fig. 7, Campbell's recommended values for the M_2 subshell are again almost entirely based on Salem's and Cooper's XES measurements. We have recalculated the M_2

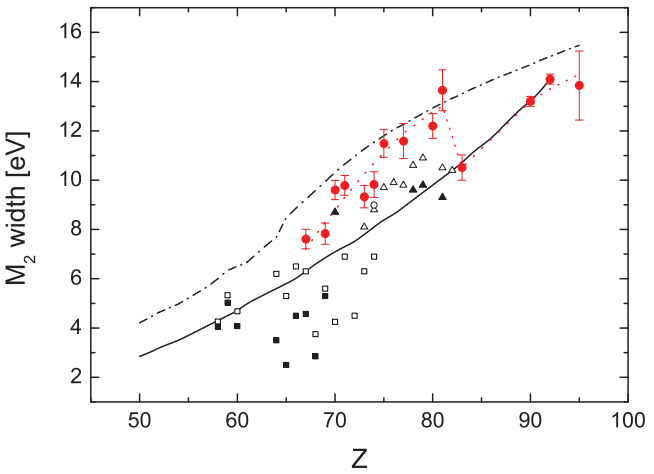

FIG. 7. (Color online) Same as Fig. 6 but for the M_2 level width. The open circle corresponds to Ref. [5]. The width of $_{67}$Ho from [4] was added to the Fribourg data (red full circles).

level widths in the region $58 \leqslant Z \leqslant 66$ using the L_1M_2 linewidths of Salem and Lee and the L_1 level widths of Raboud and we have compared the obtained results to the values extracted from the present L_1M_2 XES measurements and other previous L_1M_2 XES measurements of the Fribourg group concerning $_{67}$Ho [4], $_{80}$Hg [11], $_{90}$Th [9], and $_{92}$U [9]. From the comparison, one sees that in the region $67 \leqslant Z \leqslant 74$, Salem's data lie clearly below the Fribourg values and this may indicate, as was the case for the M_3 level width, that the whole set of M_2 level widths obtained from Salem's measurements lies too low. In addition Salem's data reveal a drop around $Z = 63$ which is neither predicted by Perkins's calculations nor by the $(Z + 1)$ approximation.

According to the $(Z + 1)$approximation, the $M_2M_4N_1$ CK transition becomes forbidden at $Z = 86$, so maybe the closing of this CK channel explains the abrupt drop in our data at $Z = 83$. Perkins calculations, however, do not predict this drop and show, on the contrary, that the $M_2M_4N_1$ CK transitions are allowed for all elements with atomic numbers $21 \leqslant Z \leqslant 100$. On the other hand, Perkins calculations predict, in contrast to the $(Z + 1)$ approximation that the $M_2M_5N_4$ CK transition becomes forbidden at $Z = 74$ and then allowed again from $Z = 79$. This may explain the small drop observed in our data at $Z = 73$ and the almost linear increase occurring between $Z = 77$ and $Z = 81$.

V. CONCLUDING REMARKS

High-resolution measurements of the L_1M_2 and L_1M_3 x-ray emission lines of $_{69}$Tm, $_{70}$Yb, $_{71}$Lu, $_{74}$W, $_{75}$Re, $_{77}$Ir, $_{81}$Tl, $_{83}$Bi, and $_{95}$Am were performed. The fluorescence x-ray spectra were produced by irradiating the targets with the bremsstrahlung of x-ray tubes. Elements up to $_{77}$Ir were measured with a Bragg-type von Hamos crystal spectrometer. As this instrument cannot be used efficiently for photon energies above about 11 keV, elements with higher atomic numbers were measured with a Laue-type DuMond crystal spectrometer.

From the fits of the measured high-resolution x-ray spectra, accurate sets of values for the energies and widths of the $L_1M_{2,3}$ transitions were obtained. Assuming for the L_1 levels the widths reported by Raboud *et al.* [4], the widths of the M_2 and M_3 atomic levels could be determined. Except for Am for which the fluorescence x-ray emission was very weak due to the tiny dimensions of the sample, present results are in general three to five times more accurate than former existing data.

The transition energies were compared to the values compiled by Deslattes *et al.* [16]. In general, a satisfactory agreement was observed, except for a few elements for which the experimental values quoted in [16] are obviously wrong. Note that for the elements investigated in the present work all values reported in [16] correspond to old measurements performed by Bearden in the late 1960s. One would like to emphasize that a very good agreement was found, however, with the theoretical MBPT transition energies that are also quoted in [16].

The results obtained from the transition widths and atomic level widths were compared to the values tabulated by Campbell and Papp [1] and to theoretical predictions of Perkins [20] based on the independent-particle model. In general, our results are significantly bigger than the values quoted in [1] and smaller than the theoretical predictions of Perkins. The sudden drops and enhancements observed in the plots of the $M_{2,3}$ level widths versus atomic number Z could be explained satisfactorily by the cutoffs and onsets of the $M_2M_4N_1$, respectively $M_3M_4N_{3,4,5}$ and $M_3M_5N_{2,3}$ CK transitions. In particular, it was found that the values of Z at which abrupt jumps were observed in the plots could be well reproduced in most cases using the semiempirical $(Z + 1)$ approximation for the calculation of the CK cutoff and onset energies.

ACKNOWLEDGMENT

The financial support of the Swiss National Science Foundation is acknowledged.

[1] J. L. Campbell and T. Papp, At. Data Nucl. Data Tables **77**, 1 (2001).
[2] S. I. Salem and P. L. Lee, Phys. Rev. A **10**, 2033 (1974).
[3] J. N. Cooper, Phys. Rev. **65**, 155 (1944).
[4] P.-A. Raboud, M. Berset, J.-Cl. Dousse, and Y. P. Maillard, Phys. Rev. A **65**, 022512 (2002).
[5] J. Wigger, Ph.D. thesis, University of Muenster, Germany, 1985.
[6] A.-M. Vlaicu, T. Tochio, T. Ishizuka, D. Ohsawa, Y. Ito, T. Mukoyama, A. Nisawa, T. Shoji, and S. Yoshikado, Phys. Rev. A **58**, 3544 (1998).
[7] P. Amorim, L. Salgueiro, F. Parente, and J. G. Ferreira, J. Phys. B **21**, 3851 (1988).
[8] J. Hoszowska, J.-Cl. Dousse, and C. Rhême, Phys. Rev. A **50**, 123 (1994).
[9] P.-A. Raboud, J.-Cl. Dousse, J. Hoszowska, and I. Savoy, Phys. Rev. A **61**, 012507 (1999).
[10] U. Werner and W. Jitschin, Phys. Rev. A **38**, 4009 (1988).
[11] Y.-P. Maillard, J.-Cl. Dousse, and J. Hoszowska, Eur. Phys. J. D **57**, 155 (2010).
[12] J.-Cl. Dousse and J. Hoszowska, Phys. Rev. A **56**, 4517 (1997).
[13] J. Hoszowska, J.-Cl. Dousse, J. Kern, and C. Rhême, Nucl. Instrum. Methods. Phys. Res., Sect. A **376**, 129 (1996).
[14] R. D. Deslattes and E. G. Kessler, in *Atomic Inner-Shell Physics*, edited by B. Crasemann (Plenum, New York, 1985), p. 181.
[15] E. G. Kessler, R. D. Deslattes, D. Girard, W. Schwitz, L. Jacobs, and O. Renner, Phys. Rev. A **26**, 2696 (1982).
[16] R. D. Deslattes, E. G. Kessler, P. Indelicato, L. de Billy, E. Lindroth, and J. Anton, Rev. Mod. Phys. **75**, 35 (2003).
[17] O. Mauron, J.-Cl. Dousse, S. Baechler, M. Berset, Y.-P. Maillard, P.-A. Raboud, and J. Hoszowska, Phys. Rev. A **67**, 032506 (2003).
[18] J. A. Bearden, Rev. Mod. Phys. **39**, 78 (1967).
[19] J. Desclaux, At. Data Nucl. Data Tables **12**, 311 (1973).

[20] S. T. Perkins, D. E. Cullen, M. H. Chen, J. H. Hubbell, J. Rathkopf, and J. Scofield, Lawrence Livermore National Laboratory Report UCRL-50400, Vol. 30, 1991 (unpublished).
[21] E. J. McGuire, Phys. Rev. A **5**, 1043 (1972).
[22] M. H. Chen, B. Crasemann, and H. Mark, Phys. Rev. A **27**, 2989 (1983).
[23] M. H. Chen, B. Crasemann, and H. Mark, Phys. Rev. A **21**, 449 (1980).
[24] D. Coster and R. D. L. Kronig, Physica **2**, 13 (1935).
[25] W. Bambynek, B. Crasemann, R. W. Fink, H. U. Freund, H. Mark, C. D. Swift, R. E. Price, and P. V. Rao, Rev. Mod. Phys. **44**, 716 (1972).
[26] J. H. Scofield, Phys. Rev. A **9**, 1041 (1974).
[27] M. Ohno, Phys. Rev. B **29**, 3127 (1984).
[28] R. L. Cohen, G. K. Wertheim, A. Rosencwaig, and H. J. Guggenheim, Phys. Rev. B **5**, 1037 (1972).
[29] J. L. Campbell and T. Papp, X-Ray Spectrom. **24**, 307 (1995).
[30] J. N. Cooper, Phys. Rev. **61**, 234 (1942).
[31] S. Salem and P. Lee, At. Data Nucl. Data Tables **18**, 233 (1976).
[32] L. Storm and H. I. Israel, At. Data Nucl. Data Tables **7**, 565 (1970).
[33] N. Mårtensson and R. Nyholm, Phys. Rev. B **24**, 7121 (1981).